Electronic Supplementary Material (ESI) for Journal of Materials Chemistry C.
This journal is © The Royal Society of Chemistry 2022

Electronic Supporting Information Available

C_1-symmetrical [Ir(C^N^1)(C^N^2)(N^O)]-*tris*-heteroleptic Ir(III)-complex with one strong N^O-ancillary π-donor for efficient all-solution-processed near-infrared (NIR) polymer light-emitting diodes (PLEDs)

Yan Zhang,‡[a] Baowen Wang,‡[a] Jiaxiang Liu,[a] Xingqiang Lü,[a,*] Wentao Li,[a,b,*] Guorui Fu,[a,b*] and Wai-Yeung Wong[b,*]

Supporting information

Materials and characterization

All reagents were received from Sigma Aldrich and used without further purification. All solvents unless otherwise stated were degassed and stored over 3 Å activated molecular sieves prior to use. All manipulations of air and water sensitive compounds were carried out under dry N_2 using the standard Schlenk line techniques.

Elemental analysis (EA) was performed on a Perkin-Elmer 240C elemental analyzer. Fourier Transform Infrared (FT-IR) spectra were recorded on a Nicolet Nagna-IR 550 spectrophotometer in the region 4000-400 cm^{-1} using KBr pellets. ^{1}H NMR spectra were recorded on a JEOL EX 400 spectrometer with $SiMe_4$ as internal standard in $CDCl_3$ or DMSO-d_6 at room temperature. Electro-spray ionization mass spectrometry (ESI-MS) was performed on a Finnigan LCQ^{DECA} XP HPLC-MS_n mass spectrometer with a mass to charge

(*m/z*) range of 4000 using a standard electro-spray ion source and CH_2Cl_2 as the solvent. Electronic absorption spectra in the UV-visible-NIR region were recorded with a Cary 300 UV spectrophotometer. Visible or NIR emission and excitation spectra were collected by a combined fluorescence lifetime and steady-state spectrometer (FLS-980, Edinburgh) with a 450 W Xe lamp. Excited-state decay times were obtained by the same spectrometer but with a μF900 Xe lamp. The quantum yield (Φ_{PL}) in solution was measured with free-base tetraphenylporphyrin (Φ_r = 0.13 in toluene solution at 298 K) as the standard.[S1] The solution was degassed by three freeze-pump-thaw circles. The following equation 1 was used to calculate the quantum yields:

$$\Phi_s = \Phi_r \times [(n_s^2 \times A_r \times I_s)/(n_r^2 \times A_s \times I_r)] \quad (1)$$

where Φ_s is the quantum yield of the sample, Φ_r is the quantum yield of the reference, n_s is the refractive index of the sample, n_r is the refractive index of the reference, A_s and A_r are the absorbance of the sample and the reference at the wavelength of excitation (355 nm), respectively, and the I_s and I_r are the integrated areas of emission bands of the sample and the reference from 600 to 900 nm, which were recorded by a red photomultiplier tube (PMT) detector. Thermal properties were characterized using thermogravimetric (TG) analyses on a NETZSCH TG 209 instrument under a flow of nitrogen at a heating rate of 10 °C/min.

Synthesis of the HC^N[1] ligand Hiqbt (1-(benzo[*b*]-thiophen-2-yl)-isoquinoline)

The HC^N[1] ligand **Hiqbt** was synthesized from the improved Suzuki coupling reaction of 2-chloro-isoquinoline[S2] (instead of 2-bromo-isoquinoline[S3]) with benzo[*b*]thien-2-yl boronic acid. A mixture of 2-chloro-isoquinoline (0.653 g, 4.0 mmol) and benzo[*b*]thien-2-y boronic acid (0.713 g, 4.0 mmol) was dissolved into absolute mixed solvents of toluene-EtOH (60 mL; v/v = 2:1) under a N_2 atmosphere. Then an aqueous solution (20 mL) of Na_2CO_3 (2 M) was added, and the mixture was degassed by a N_2 flow. Anhydrous $Pd(PPh_3)_4$ (190 mg, 0.2 mmol; 5 mol%) was added to the reaction mixture which was then heated at 85 °C for 48 h. The complete consumption of reagents was monitored by thin-layer chromatography (Hexane/AcOEt, v/v = 9:1). After cooling to room temperature, the organic phase was washed with brine and extracted with absolute CH_2Cl_2 (3×20 mL) three times. The combined organic phase was dried over anhydrous Na_2SO_4, and further purified with flash-column chromatography on silica gel (Hexane/AcOEt, v/v = 9:1), affording an off-white solid. For the **Hiqbt**: Yield: 0.762 g (73%). Calcd for $C_{17}H_{11}NS$: C, 78.13; H, 4.24; N, 5.36%. Found: C, 78.05; H, 4.36; N, 5.29%. ^{1}H NMR (400 MHz, DMSO-d_6): δ (ppm) 8.70 (d, 1H, -Py), 8.61 (d, 1H, -Ph), 8.19 (s, 1H, -Th), 8.11 (d, 1H, -Ph), 8.06 (m, 1H, -Ph), 8.02 (m, 1H, -Py), 7.88 (m, 2H, -Ph), 7.81 (t, 1H, -Ph), 7.46 (m, 2H, -Ph).

Synthesis of the N^OH ancillary ligand Hpbi (2-(1*H*-benzo[*b*]imidazol-2-yl)-phenol)

The N^OH-ancillary π-donor ligand **Hpbi** was synthesized according to an improved synthetic procedure as the literature.[S4] To a solution of $NaHSO_3$ (1.040 g, 10 mmol) in absolute DMF (20 mL), salicylaldehyde (1.122 g, 1.066 mL, 10.0 mmol) was added slowly and the resulting

mixture was continuously stirred at room temperature for 0.5 h. subsequently, 1,2-diaminobenzene (0.440 g, 2 mmol) was added, and the mixture's colour was changed from yellow to reddish-brown during reaction under refluxing at 80 °C for 12 h. After cooling to room temperature, excess D. I. water (100 mL) was poured into the mixture, and the white suspension was filtrated, affording to an off-white crude product. The crude powder was further re-crystallized with absolute EtOH to get off-white polycrystalline. For the **Hpbi**: Yield: 1.682 g (80%). Calc. for $C_{13}H_{10}N_2O$: C, 74.27; H, 4.79; N, 13.33%. Found: C, 74.21; H, 4.86; N, 13.30%. ^{1}H NMR (400 MHz, DMSO-d_6): δ (ppm) 13.18 (2H, -NH/-OH), 8.06 (m, 1H, -Ph), 7.67 (m, 2H, -Ph), 7.39 (t, 1H, -Ph), 7.29 (d, 2H, -Ph), 7.03 (m, 2H, -Ph).

Cyclic voltammetry (CV) measurement

Electro-chemical measurements were made using a Princeton Applied Research model 2273A potentiostat at a scan rate of 100 mV/s. A conventional three-electrode configuration consisting of a glassy carbon working electrode, a Pt-sheet counter electrode, and a Pt wire reference electrode was used. The supporting electrolyte was 0.1 M tetrabutylammonium tetrafluoroborate ($[Bu_4N]BF_4$) in anhydrous MeCN. Ferrocene was added as a calibrant after each set of measurements, and all potentials reported are quoted with reference to the Fc^+/Fc couple. The oxidation (E_{ox}) and reduction (E_{red}) potentials were used to determine the HOMO and LUMO energy levels using Equations (2) and (3),[S5] respectively,

$$E_{HOMO} = -(E_{OX}^{on} + 4.4)\ eV \quad (2)$$

$$E_{LUMO} = E_{HOMO} + E_g^{OPT}\ eV \quad (3)$$

where E_{OX}^{on} is the recorded onset oxidation potential of the complex, and E_g^{OPT} is the energy band gap estimated from the low-energy edge of the absorption spectra from the samples. The HOMO and LUMO energy levels for the other used materials were obtained from the literatures.[S6]

Fabrication and testing of the all-solution-processed NIR-PLEDs ASP-Type-I-A-1/2 doped with [(iqbt)$_2$(pbi)] (1) or [(iqbt)(btp)(pbi)] (2)

Each of the all-solution-processed **NIR-PLEDs ASP-Type-I-A-1/2** was fabricated on ITO (Indium tin oxide) coated glass substrates with a sheet resistance of 20 Ω per square. Patterned ITO coated glass substrates were washed with acetone, detergent, D. I. water and isopropanol in an ultrasonic bath. After being exposed under oxygen plasma for 20 min, PEDOT:PSS from water solution was spin-coated (at 4800 rpm) on the substrate followed by drying in a vacuum oven at 130 °C for 30 min, giving a film of 50 nm in thickness. The chlorobenzene solution (30 mg/mL) of the mixture of PVK, OXD7 and one of the [(iqbt)$_2$(pbi)] (**1**) and [(iqbt)(btp)(pbi)] (**2**) as the emitting layer (EML) was prepared under an N_2 atmosphere and spin-coated (at 4000 rpm) on the PEDOT:PSS layer with a thickness of 120 nm. Finally, a thin layer (1 nm) of LiF followed by Al capping layer (100 nm) was deposited onto the substrate under vacuum (5×10^{-6} Pa). Current density-voltage (*J*-*V*) characteristics were collected using a Keithley 2400 source meter equipped with a calibrated silicon photodiode. The NIR EL irradiance (*R*) was measured through a PR735 Spectra Scan spectrometer. The external quantum efficiency (η_{EQE}) of the NIR emission was obtained by

measuring the irradiance in the forward direction and assuming the external emission profile to Lambertian.

Fabrication and testing of the all-solution-processed NIR-PLEDs ASP-Type-I-B-1/2 doped with [$(iqbt)_2$(pbi)] (1) or [(iqbt)(btp)(pbi)] (2)

Similarly using a mixture of the bipolar co-host and the the [Ir$(iqbt)_2$(pbi)] (**1**) or the [Ir(iqbt)(btp)(pbi)] (**2**) with a stipulated 5 wt% doping content as the EML, their **ASP-Type-I-B-1/2** were configured with ITO/PEDOT:PSS (50 nm)/PVK:OXD7:Ir(III)-complex (120 nm)/Ba (7 nm)/Al (100 nm). That is, a thin layer (7 nm) of Ba followed by Al capping layer (100 nm) as the cathode was deposited onto the substrate under vacuum (5×10^{-6} Pa). The difference between the **ASP-Type-I-A-1/2** and the **ASP-Type-I-B-1/2** is the usage of Ba (7 nm)/Al (100 nm) instead of LiF (1 nm)/Al (100 nm) as the cathode, respectively. Details of testing for the **ASP-Type-I-B-1/2** were in the same way as for **ASP-Type-I-A-1/2**, respectively.

References

S1 J. H. Palmer, A. C. Durrell, Z. Gross, J. R. Winkler and H. B. Gray, *J. Am. Chem. Soc.*, 2010, **132**, 9230-9231.

S2 G. R. Fu, H. Zheng, Y. N. He, W. T. Li, X.Q. Lü and H. S. He, *J. Mater. Chem. C*, 2018, **6**, 10589-10596.

S3 S. Kesarkar, W. Mróz, M. Penconi, M. Pasini, S. Destri, M.Cazzaniga, D. Ceresoli, P. R. Mussini, C. Baldoli, U. Giovanella and A. Bossi, *Angew. Chem. Int. Ed.*, 2016, **55**, 2714-2718.

S4 M. Martínez-Alonso, N. Busto, L. D. Aguirre, L. Berlanga, M. C. Carrión, J. V. Cuevas, A. M. Rodríguez, A. Carbayo, B. R. Manzano, E. Ortí, F. A. Jalón, B. García and G. Espino, *Chem. Eur. J.* 2018, **24**, 17523-17537.

S5 H. Y. Chen, C. T. Chen and C. T. Chen, *Macromolecules,* 2010, **43**, 3613-3623.

S6 E. Zysman-Colman, S. S. Ghosh, G. Xie, S. Varghese, M. Chowdhury, N. Sharma, D. B. Cordes, A. M. Z. Slawin and I. D. W. Samuel, *ACS Appl. Mater. & Interfaces,* 2016, **8**, 9247-9253.

Table S1 The photophysical property comparison between the *bis*-heteroleptic Ir(III)-complexes [Ir(iqbt)$_2$(pbi)] (**1**)/[Ir(btp)$_2$(pbi)] (**3**) and the *tris*-heteroleptic Ir(III)-complex [Ir(iqbt)(btp)(pbi)] (**2**) with previously reported *fac*-[Ir(iqbt)$_3$], [Ir(iqbt)$_2$(L^X)] and [Ir(iqbt)(C^N^2)(L^X)] analogues in degassed CH_2Cl_2 solution at RT or 77 K, respectively

Comp.	**Absorption**[a]		**Emission** (RT)[a]						**Emission** (77 K)[a]		**Energy level**	
-Ref	λ_{abs} (nm)	λ_{ex} (nm)	λ_{em} (nm)	S_M[c]	τ (μs)	Φ_{PL}	k_r[b] (s^{-1})	k_{nr}[b] (s^{-1})	λ_{em} (nm)	S_M[c]	HOMO[d] (eV)	LUMO[d] (eV)
1	227, 292, 369, 534	556	712, 775(sh)	0.21	0.59	0.29	4.9×10^5	1.20×10^6	711, 771(sh)	0.24	-4.62 (-5.16)	-1.96 (-3.06)
2	226, 286, 357, 540	545	714, 782(sh)	0.20	0.49	0.36	7.3×10^5	1.31×10^6	710, 777(sh)	0.19	-4.57 (-5.09)	-2.02 (-3.01)
3	233, 294, 384, 426	444	614, 663(sh)	0.40	-[e]	0.58	-[e]	-[e]	607, 659(sh)	0.43	-4.58	-1.67
fac-[Ir(iqbt)$_3$]-[21d]	-[e]	690	-[e]	1.77	0.15	-	-	-	-	-	-	
[Ir(iqbt)$_2$(hpa)]-[18b]	-[e]			2.13	0.13	0.6×10^5	0.4×10^5	704	-	-4.95 (-5.47)	-2.12 (-3.30)	
[Ir(iqbt)$_2$(hpa-BF$_2$)]-[18b]	-[e]	700	-	0.76	0.08	1.1×10^5	1.2×10^6	696	-	-5.19 (-5.38)	-2.33 (-3.19)	
[Ir(iqbt)$_2$(dpm)]-[21a]	-[e]	710	-	1.40	0.16	1.1×10^5	6.0×10^5	-	-	(-5.15)	(-2.71)	
[Ir(iqbt)$_2$(tta)]-[21a]	-e	704	-	0.76	0.07	0.97×10^5	1.3×10^6	-	-	(-5.31)	(-2.96)	
[Ir(iqbt)$_2$(dtdk)]-[21a]	-[e]	707	-	1.44	0.14	0.97×10^5	6.0×10^5	-	-	(-5.19)	(-2.76)	
[Ir(iqbt)$_2$(vb-bpy)]-[19c]	-[e]	693	-	0.25	0.19	7.6×10^5	-	-	0.98	-4.68	-1.88	
[Ir(iqbt)(dFppy)(acac)]-[19a]	-[e]	703	0.29	0.30	0.18	6.0×10^5	2.7×10^6	-	-	-4.89	-1.89	
[Ir(iqbt)(ppy)(acac)]-[19a]	-[e]	715	0.32	0.42	0.26	6.1×10^5	1.8×10^6	-	-	-4.73	-1.79	

[Ir(iqbt)(dpqx)(acac)]-[19a]	-[e]	707	0.38	0.45	0.28	6.2×10^5	1.6×10^6	-	-	-4.83	-2.16
[Ir(iqbt)(ppy)(pic)]-[19b]	-[e]	698	0.31	0.34	0.27	7.9×10^5	2.1×10^6	698	0.28	-4.95	-1.98
[Ir(iqbt)(ppy)(Br-pic)]-[19b]	-[e]	696	0.31	0.35	0.21	2.3×10^5	2.1×10^6	696	0.30	-5.09	-2.05

[a]Measured in degassed CH_2Cl_2 solution;

[b]$k_r = \Phi_{PL}/\tau$, $k_{nr} = (1 - \Phi_{PL})/\tau$ on the assumption that $\Phi_{ISC} = 1$ (ISC = intersystem crossing);

[c]Huang–Rhys factor (S_M) is calculated from the peak heights and energies of (0-0) and (0-1) band, $S_M = (I_{0-1}/I_{0-0})\,(\bar{\nu}_{0\text{-}0}/\bar{\nu}_{0\text{-}1})$;

[d]HOMO and LUMO levels are obtained from theoretical calculations and electrochemical determinations, respectively;

[e]That is not be determined or compared.

Table S2 Frontier orbital energy and electron density distribution for the *bis*-heteroleptic Ir(III)-complexes **1/3** and the *tris*-heteroleptic Ir(III)-complex **2** on the basis of their optimized S_0 geometries

Complex	MOs	Contribution of d_π and π orbitals of ligands to Mos (%)				Main configuration of $S_0 \rightarrow S_1$ excitation, λ_{cal} (nm), f	Main configuration of $S_0 \rightarrow T_1$ excitation; λ_{cal} (nm)
		Ir	**iqbt-1**	**iqbt-2**	**pbi**	HOMO → LUMO (89.19%),	HOMO → LUMO (73.71%);
	LUMO+2	0.59	0.90	1.97	96.54	546 nm (2.272 eV),	HOMO-2 → LUMO+1 (13.66%);
	LUMO+1	4.70	22.79	71.52	0.99	0.0316	708 nm (1.750 eV)
1	LUMO	5.63	70.48	22.42	1.47		
	HOMO	24.82	33.42	34.77	6.99		
	HOMO-1	10.85	2.03	8.73	78.39		
	HOMO-2	0.46	50.04	46.45	3.05		
		Ir	**iqbt**	**btp**	**pbi**	HOMO → LUMO (96.92%),	HOMO → LUMO (75.91%);
	LUMO+2	1.02	0.93	1.53	96.52	552 nm (2.246 eV),	HOMO-2 → LUMO (16.93%);
	LUMO+1	4.88	0.93	92.44	1.75	0.0567	715 nm (1.733 eV)
2	LUMO	5.29	92.22	1.01	1.48		
	HOMO	23.57	32.49	22.21	21.73		
	HOMO-1	10.22	3.77	23.58	62.43		
	HOMO-2	1.17	51.51	42.72	4.60		
		Ir	**btp-1**	**btp-2**	**pbi**	HOMO → LUMO (86.15%);	HOMO → LUMO (63.92%);
	LUMO+2	0.46	4.38	1.32	93.84	HOMO → LUMO+1	HOMO-2 → LUMO (17.13%),
	LUMO+1	5.05	92.95	0.32	1.68	(10.00%);	598 nm (2.074 eV)
3	LUMO	5.24	0.44	92.21	2.11	479 nm (2.588 eV),	
	HOMO	27.10	31.54	30.17	11.19	0.0407	
	HOMO-1	10.92	11.47	2.72	74.88		
	HOMO-2	1.13	45.48	50.79	2.60		

λ_{cal}, and f denote the calculated emission wavelength, and oscillator strength, respectively. The oscillator strength of $S_0 \rightarrow T_1$ is zero owing to the spin-forbidden character of the singlet-triplet transition under TD-DFT calculations in the Gaussian program with no consideration of spin orbital coupling.

Table S3 Frontier orbital energy and electron density distribution for the *bis*-heteroleptic Ir(III)-complexes **1/3** and the *tris*-heteroleptic Ir(III)-complex **2** on the basis of their optimized T_1 geometries

Complex	MOs	Contribution of d_π and π orbitals of ligands to Mos (%)				Main configuration of $T_1 \rightarrow S_0$ emission, λ_{cal} (nm)[b]
		Ir	**iqbt-1**	**iqbt-2**	**pbi**	HOMO-2 → LUMO+1 (14.10%);
	LUMO+2	0.61	1.01	2.04	96.34	HOMO → LUMO (75.41%);
	LUMO+1	5.18	27.77	66.01	1.04	795 nm
1	LUMO	5.96	65.17	27.27	1.60	
	HOMO	23.44	32.46	38.67	5.43	
	HOMO-1	9.39	1.88	9.71	79.02	
	HOMO-2	0.80	52.91	41.87	4.42	
2		**Ir**	**iqbt**	**btp**	**pbi**	HOMO-2 → LUMO (12.57%);
	LUMO+2	0.96	0.70	1.92	96.42	HOMO → LUMO (84.03%);
	LUMO+1	4.92	0.56	92.66	1.86	908 nm
	LUMO	6.48	91.16	0.68	1.68	
	HOMO	20.72	49.17	16.29	13.82	
	HOMO-1	8.65	3.87	17.06	70.42	
	HOMO-2	2.06	40.18	52.79	4.97	
3		**Ir**	**btp-1**	**btp-2**	**pbi**	HOMO-2 → LUMO+1 (10.49%);
	LUMO+2	0.55	6.27	1.28	91.90	HOMO → LUMO (82.14%);
	LUMO+1	7.13	52.02	37.41	3.44	704 nm
	LUMO	4.58	39.57	54.18	1.67	
	HOMO	26.30	35.19	32.29	6.22	
	HOMO-1	8.21	11.98	2.65	77.16	
	HOMO-2	0.99	40.81	49.77	8.43	

[a]HOMO → LUMO denotes the transition from HOMO to LUMO. λ_{cal}, and *f* denote the calculated emission wavelength, and oscillator strength, respectively. The oscillator strength of $T_1 \rightarrow S_0$ is zero owing to the spin-forbidden character of the singlet-triplet transition under TD-DFT calculations in the Gaussian program with no consideration of spin-orbital coupling.

Table S4 The calculated orbital transition analyses for the *bis*-heteroleptic Ir(III)-complexes **1/3** and the *tris*-heteroleptic Ir(III)-complex **2** by TD-DFT calculations with the IFCT analyses at the B3LYP level

Complex	State	λ (nm)	*E* (eV)	Oscillator (*f*)	transition (contrib.)	Assignment (%)			
1	$S_0 \rightarrow S_1$	546	2.27	0.0316	HOMO → LUMO (73.71%); HOMO-2 → LUMO+1 (13.66%); HOMO-2 → LUMO (4.53%)	^{1}ILCT	31.286	^{1}MC	1.357
						^{1}MLCT	23.463	^{1}LMCT	4.111
						^{1}LLCT	39.782		
	$S_0 \rightarrow T_1$	708	1.75	0.0000	HOMO → LUMO (89.19%); HOMO → LUMO+1 (7.81%)	^{3}ILCT	41.811	^{3}MC	1.134
						^{3}MLCT	19.63	^{3}LMCT	4.327
						^{3}LLCT	41.811		
	$T_1 \rightarrow S_0$	795	1.56	0.0000	HOMO → LUMO (75.41%); HOMO-2 → LUMO+1 (14.10%); HOMO → LUMO+1 (2.47%)	^{3}ILCT	34.677	^{3}MC	1.157
						^{3}MLCT	18.569	^{3}LMCT	4.709
						^{3}LLCT	40.888		
2	$S_0 \rightarrow S_1$	552	2.25	0.0567	HOMO → LUMO (96.92%)	^{1}ILCT	30.508	^{1}MC	1.247
						^{1}MLCT	22.32	^{1}LMCT	4.046
						^{1}LLCT	41.881		
	$S_0 \rightarrow T_1$	715	1.73	0.0000	HOMO → LUMO (75.91%); HOMO-2 → LUMO (16.92%); HOMO-1 → LUMO (2.70%)	^{3}ILCT	62.595	^{3}MC	1.122
						^{3}MLCT	20.07	^{3}LMCT	4.171
						^{3}LLCT	12.043		
	$T_1 \rightarrow S_0$	908	1.36	0.0000	HOMO → LUMO (84.03%); HOMO-2 → LUMO (12.57%)	^{3}ILCT	68.664	^{3}MC	0.991
						^{3}MLCT	14.309	^{3}LMCT	5.485
						^{3}LLCT	10.552		
3	$S_0 \rightarrow S_1$	479	2.59	0.0407	HOMO → LUMO (86.15%); HOMO → LUMO+1 (10.00%)	^{1}ILCT	28.522	^{1}MC	1.31
						^{1}MLCT	25.791	^{1}LMCT	3.525
						^{1}LLCT	40.851		
	$S_0 \rightarrow T_1$	598	2.07	0.0000	HOMO → LUMO (63.91%); HOMO-2 → LUMO (17.13%); HOMO → LUMO+1 (7.81%); HOMO-2 → LUMO+1 (2.13%)	^{3}ILCT	49.102	^{3}MC	1.246
						^{3}MLCT	21.63	^{3}LMCT	41.99
						^{3}LLCT	23.823		
	$T_1 \rightarrow S_0$	704	1.76	0.0000	HOMO → LUMO (82.14%); HOMO-2 → LUMO+1 (10.49%)	^{3}ILCT	32.719	^{3}MC	1.142
						^{3}MLCT	22.292	^{3}LMCT	3.729
						^{3}LLCT	40.117		

Table S5 The transition dipole moments $\Delta\mu$ comparison for the *bis*-heteroleptic Ir(III)-complexes **1/3** and the *tris*-heteroleptic Ir(III)-complex **2** with upon DFT calculations based on their corresponding optimized T_1 and S_0 states

Complex	**State**	***x***	***y***	***z***	$\left\vert\vec{\mu}\right\vert$ (D)	θ (°)	$\left\vert\Delta\vec{\mu}\right\vert$ (^{1}T-^{0}S) (D)
1	S_0	-0.7839	3.7813	0.9351	3.97	2.7	0.26
	T_1	-0.7807	3.5508	1.0553	3.78		
2	S_0	-3.8982	-1.5599	1.7902	4.56	35.6	2.77
	T_1	-2.0134	-3.5862	1.8003	4.49		
3	S_0	4.4267	0.8600	0.1655	4.51	5.1	0.67
	T_1	3.9382	0.4466	-0.0242	3.96		

Figure S1 The ^{1}H NMR spectra of the HC^N (**Hiqbt**-HC^N[1]; **Hbtp**-HC^N[2]) and N^OH-**Hpbi** ligands and their Ir(III)-complexes **1**-**3** in DMSO-d_6 at room temperature, respectively.

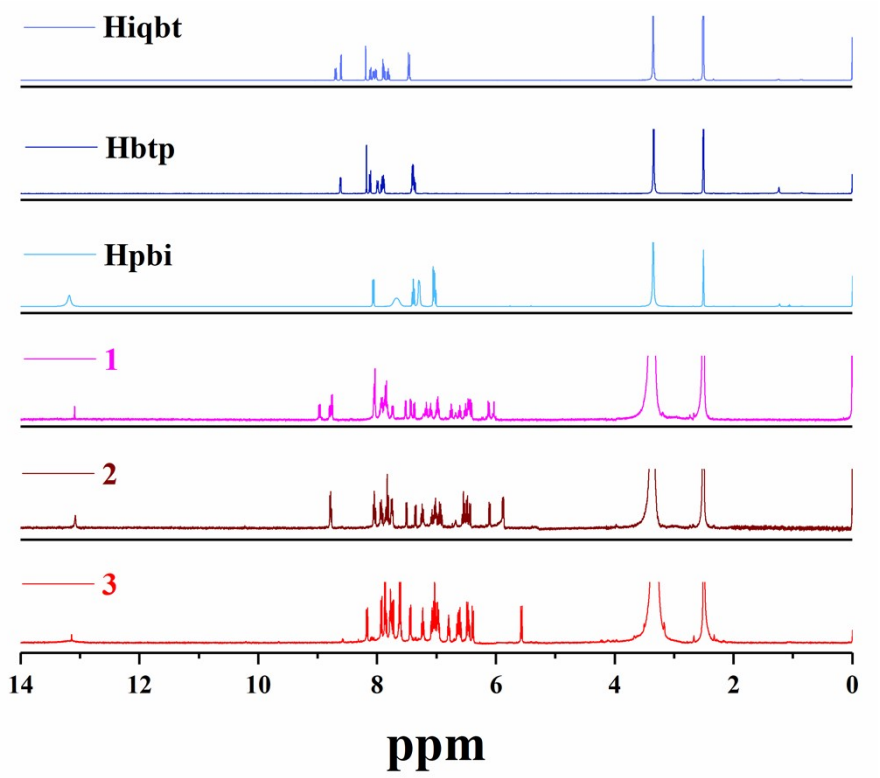

Figure S2 The thermogravimetric analysis (TG) curves for the Ir(III)-complexes **1**-**3**, respectively.

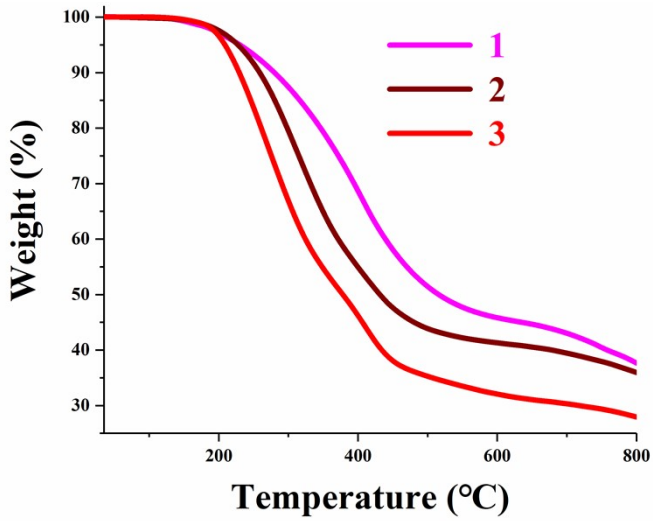

Figure S3 The normalized UV-visible absorption spectra of the HC^N (**Hiqbt**-HC^N[1]; **Hbtp**-HC^N[2]) and N^OH-**Hpbi** ligands in degassed CH_2Cl_2 solutions at room temperature, respectively.

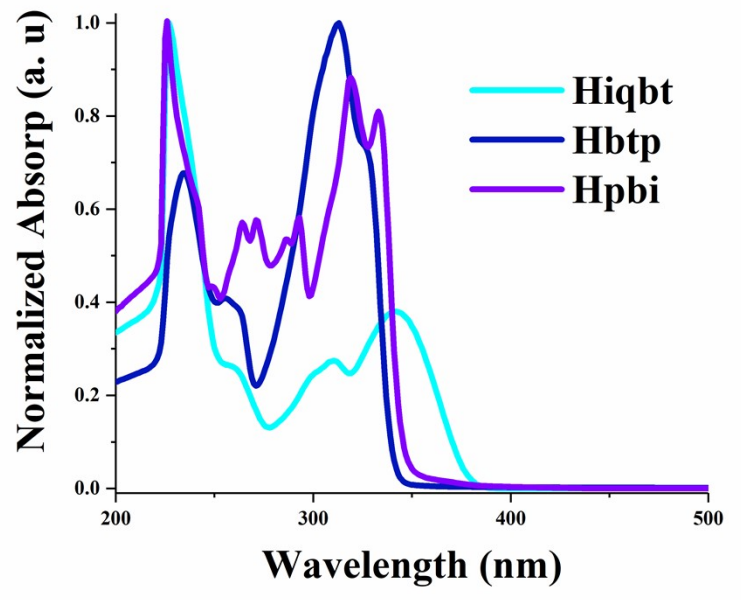

Figure S4 The normalized emission spectra of the HC^N (**Hiqbt**-HC^N[1]; **Hbtp**-HC^N[2]) and N^OH-**Hpbi** ligands in degassed CH_2Cl_2 solutions at room temperature, respectively.

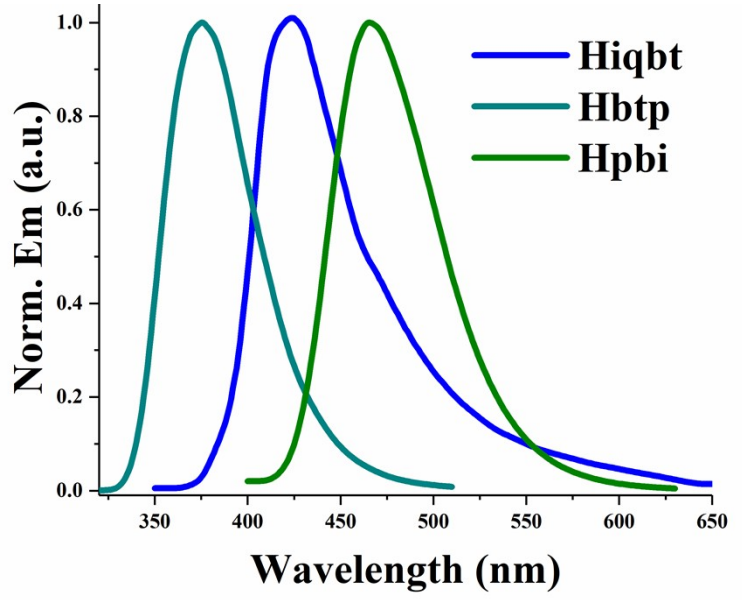

Figure S5 The normalized emission spectra of Ir(III)-complexes **1**-**3** in degassed CH_2Cl_2 solutions at 77 K, respectively.

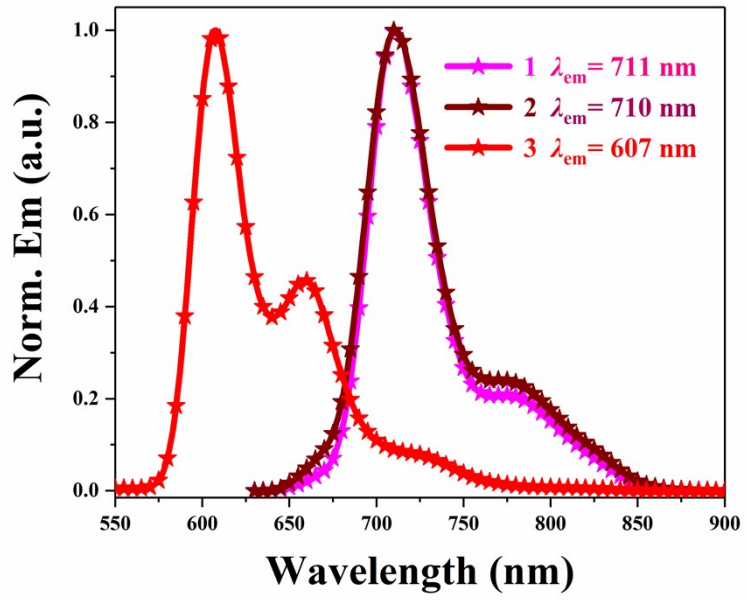

Figure S6 Chemical structure and TDMs (transition dipole moments) of the *bis*-heteroleptic Ir(III)-complex [Ir(btp)$_2$(pbi)] (**3**) by DFT calculations.

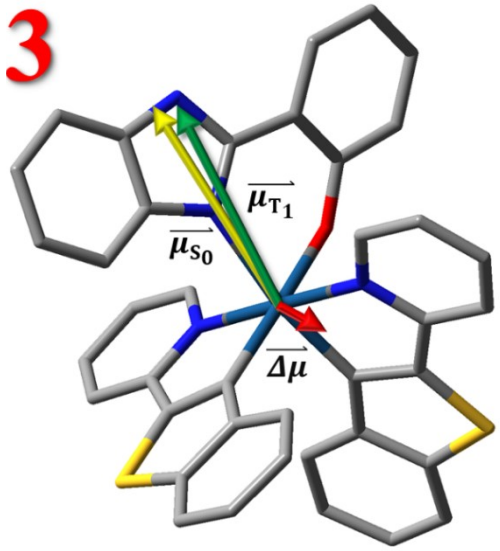

Figure S7 The cyclic voltammogram (CV) results of the Ir(III)-complexes **1**-**2** recorded versus Fc^{+}/Fc in solution at room temperature under a N_2 atmosphere (scan rate = 100 mV/s), respectively.